Available online at www.sciencedirect.com
SCIENCE DIRECT®
Polymer 45 (2004) 1665–1678
polymer
www.elsevier.com/locate/polymer

Effects of viscosity ratio and composition on development of morphology in chaotic mixing of polymers

Sadhan C. Jana*, Madhusudan Sau

Department of Polymer Engineering, University of Akron, Akron, OH 44325-0301, USA

Received 4 August 2003; received in revised form 2 December 2003; accepted 5 December 2003

Abstract

This study investigated the effects of viscosity ratio (p) and composition on morphology development in an immiscible polymer system mixed under chaotic flow conditions. It was seen that morphology of the dispersed phase developed through a widely accepted route involving transitions from lamellas to fibrils and to droplets. It was found in experiments with $p \geq 1$ that the dispersed phase converted into droplets very rapidly with narrow droplet size distribution when $p \sim 1$. For higher values of p, the speed of morphological transitions slowed down, the droplet size distribution became wider, and much larger droplets were formed. Similar effects were observed at higher concentration of the dispersed phase. No self-similar scaling behavior was observed in the droplet size distribution, which can be attributed to the lack of self-similarity in the breakup of lamellas into fibrils.

Keywords: Chaotic mixing; Morphology; Self-similar

1. Introduction

The morphology of immiscible polymer blends results from an interplay of viscous and interfacial forces and associated flow kinematics in the mixing device. *Processing parameters*, such as rates of shear, total strain, and frequency of fluid elements reorientation and *material parameters*, such as interfacial tension, viscosity, and relaxation modulus, along with *mixer designs* and composition dictate the overall morphology. Lamellas, fibrils, droplets, and their combinations are common morphological forms in immiscible polymer blends [1–8].

Morphology development in immiscible polymers occurs through transformation of dispersed domains into lamellas, fibrils, and finally to droplets [2–8]. Lamellar structures, with alternating layers of component polymers, are formed in the early stages of blending of immiscible polymers [1–3,8]. The kinematics of lamellar structure formation is similar to mixing of viscous miscible liquids; component polymers deform affinely and produce alternating, nested layers, characterized by *striation thickness* distribution along a cross-sectional plane [9]. The striation thickness of lamellas decreases with continued mixing, e.g. linearly with time in common mixing flows, such as those encountered in single and twin-screw extruders [10,11] and exponentially in chaotic mixing flows [12–20]. The lamellar structures in miscible liquids go through repetitive thinning until molecular diffusion takes over and homogenizes the system.

The lamellar structures in immiscible polymers undergo interfacial instabilities beyond a *critical lamella thickness*, whereby periodic distortions are produced in the lamellas and the lamellas eventually transform into fibrillar structures [2,8]. The fibrils, thus formed, undergo capillary instability [21–28] and generate droplets upon breakup. The newly formed droplets may repeat the same steps of breakup if the droplet capillary number (Ca) exceeds the critical capillary number (Ca_c). A pseudo-equilibrium state is reached when a somewhat stable morphology is achieved from the balance of interfacial and viscous forces and from the competing rates of breakup and coalescence of droplets [28,29].

In view of the pathway of morphology development described above, two useful features make blending by chaotic mixing attractive: [1] exponential thinning of lamellas and fibrils and [2] opportunities for creation and retention of self-similar mixing structures. Self-similarity of

* Corresponding author. Tel.: +1-330-972-8293; fax: +1-330-258-2339.
E-mail address: janas@uakron.edu (S.C. Jana).

0032-3861/$ - see front matter © 2003 Elsevier Ltd. All rights reserved.
doi:10.1016/j.polymer.2003.12.047

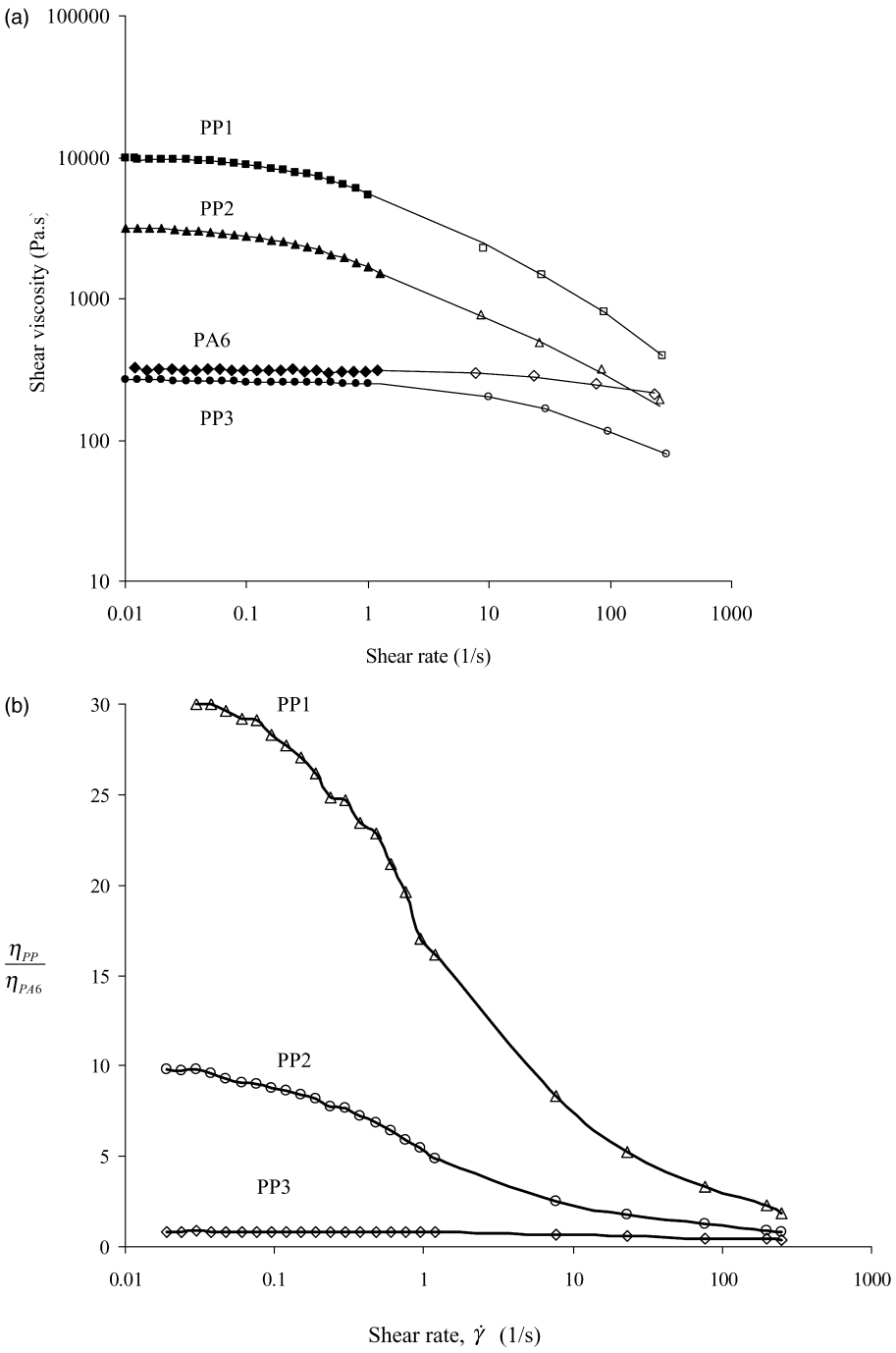

Fig. 1. (a) Shear viscosity of PP1, PP2, PP3, and PA6 at 250 °C. Filled symbols represent data from cone-plate rheometer and open symbols represent data from capillary rheometer. Solid lines represent interpolation of data points. (b). Ratio of shear viscosity of PP and PA6 at 250 °C. Solid lines represent interpolation of data points.

mixing structures produced in chaotic mixing has formed the basis of a series of investigations, e.g. scaling features in stretching distribution [30], scalability of droplet size distribution in the breakup of cylindrical liquid threads [31], hydrodynamics-aided chemical reactions [32–34], and in the analysis of mixing microstructures produced in industrial mixing devices [35,36].

Zumbrunnen and co-workers [37–41] studied blending of polymers by chaotic mixing, using two designs of batch chaotic mixing devices such as a 3-D cavity [37,38,41] and a journal bearing [39] and one continuous chaotic mixing device [40] based on a batch mixer design described in Ref. [17]. These authors produced various structures, such as lamellas, fibrils, droplets, and their combinations in the blending of polystyrene (PS) with low-density polyethylene (LDPE) [38–40], polypropylene (PP) with ethylene propylene diene monomer (EPDM) [39], and polyethylenevinyl acetate (EVA) with LDPE [37]. Even though the pathway of

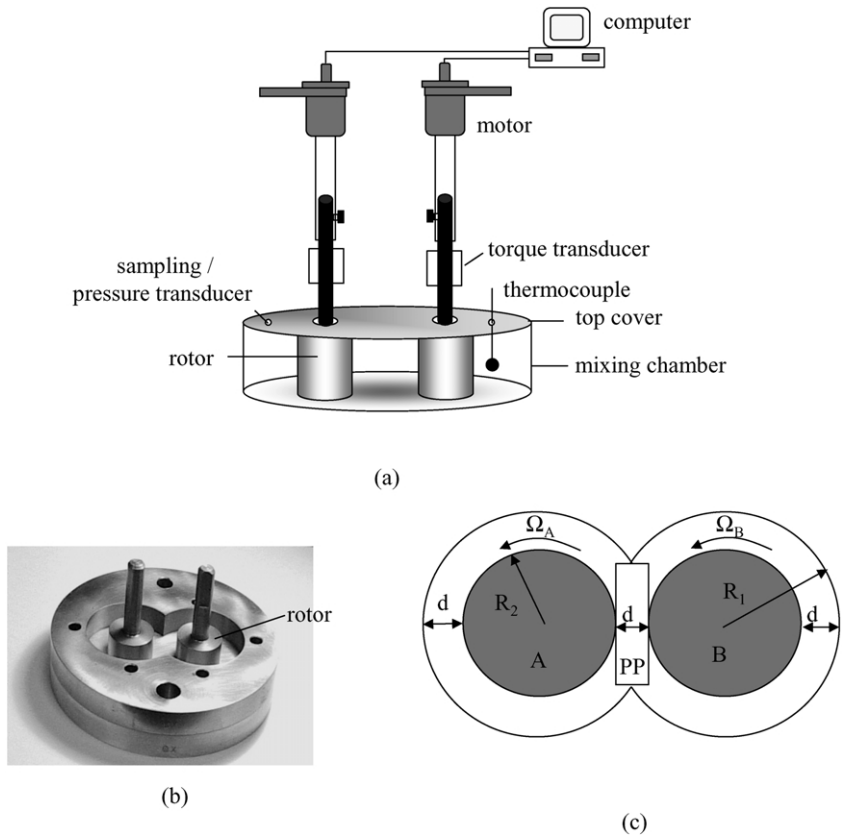

Fig. 2. (a) Experimental set-up for batch chaotic mixing. (b) Cross sectional view of the batch chaotic mixer with circular rotors. (c) R_1 is the radius of the chamber wall, R_2 is the radius of rotor, d is the gap size, Ω_A and Ω_B are angular speeds of rotors A and B.

morphology development, i.e. lamellas to fibrils to droplets, observed in these studies is similar to those observed earlier in screw extrusion [2,6], Zumbrunnen and co-workers found the lamellas and fibrils to persist over longer periods of time. Note, however, that the strain rates used by these investigators were much smaller, e.g. 0.07–2.75 (1/s) in Ref. [41], compared to typically ~50 (1/s) encountered in screw extrusion. No studies to date reported a one to one comparison of the merits of mixing of polymer products by chaotic flow and by screw extrusion at the same rates of shear.

The relationship among mixer designs, the degree of chaotic mixing, the nature of time-periodic waveforms, and the resultant morphology—although crucial for studies involving design, scale up, and optimization of batch and continuous chaotic mixing devices—have not been studied in detail. These issues must be resolved before the potential of chaotic mixing in blending of immiscible polymers can be fully realized, e.g. in the design of new products from conventional materials or in the development of value added products through creation of some unusual morphological signatures.

A thorough fundamental understanding must be developed for designing new chaotic mixing equipment or retrofitting existing ones. Some successful designs have been reported in conjunction with single-screw extruders by both industrial [42,43] and academic research groups [44–46]. Nevertheless, more work is needed to address the issues raised in the previous paragraph. Along this line, a study was undertaken in our laboratory using polypropylene (PP) and polyamide 6 (PA6) as a model polymer system. These polymers represent a combination of materials with shear-thinning, e.g. PP and Newtonian behavior, e.g. PA6, in the range of shear rates used in experiments. The effects of mixer designs, chaotic mixing parameter, θ (angular displacement per period), and the nature of waveforms of rotor motion on pathway of morphology development and droplet size distribution were studied and the results reported elsewhere [47,48]. It was found that the dispersed polymer component went through deformation to form lamellas, fibrils, and droplets as observed by other investigators [2,4–6,37–41]. The morphological transitions were expedited with the reduction of shear gap in the mixing device; the peak shear rate, however, was kept the same [47]. It was also observed that the dispersed phase more readily converted into droplets when the chaotic motion was delivered using a sine waveform with a value of $\theta = 1440°$ [48]. The other waveforms investigated were square waveform, a combination of steady motion and sine waveforms, and steady motion.

In this paper, results are presented on the effects of viscosity ratio (p) between PP and PA6 and the composition

of PP-phase on morphological transitions, droplet size distribution, and the scalability of droplet size distribution. Specifically three issues were considered in this study:

(a) The size of droplets formed relative to those permitted by the equilibrium between the interfacial and viscous forces.
(b) Comparison of the trend of droplet sizes produced for various values of p with those produced via breakup of cylindrical liquid threads [24–27] or with those reported for blending of polymers [49–54]. Note that the mean size of droplets decreases with the increase of viscosity ratio in capillary breakup of viscous threads [26,27], while the mean size increases with viscosity ratio in the blending of immiscible polymers [49,53,54].
(c) The existence of scaling behavior of droplet size distribution in view of self-similar nature of chaotic mixing.

2. Experimental section

2.1. Materials

Polyamide 6, Zytel 7301 NC010 (specific gravity 1.13), supplied by Dupont was used as the continuous phase. Three grades of homopolymer polypropylene (specific gravity 0.91), melt flow index (MFI) values of 0.7 (grade PP31S07A, PP1), 5.0 (grade PP8000-GK, PP2), and 30.0 (grade PP 51S30V, PP3) supplied by Equistar Chemicals were used as the dispersed phase. The crystalline melting points of PA6 and PP were found to be 220 and 165 °C, respectively from differential scanning calorimetry (DSC). The glass transition temperatures of three grades of PP were as follows: −20 °C (PP1), −24 °C (PP2), and −18 °C (PP3). Two blend compositions were used with 10 and 30 wt% of PP for which PA6 formed the continuous phase. The values of shear viscosity of polymers were measured by ARES Rheometrics rheometer with cone and plate configuration and Instron capillary rheometer. Fig. 1(a) presents viscosity of the component polymers at the mixing temperature of 250 °C. The ratio of shear zero-shear viscosities of PP ($\eta_{0,PP}$) and PA6 ($\eta_{0,PA6}$), $p = \dfrac{\eta_{0,PP}}{\eta_{0,PA6}}$ was 30 for PP1, 9.8 for PP2, and 0.8 for PP3. The ratios of viscosity at other shear rates are presented in Fig. 1(b). The interfacial tension (σ) between PA6 and PP was determined by thread breakup method [55] with a value of 0.0126 N m^{-1} at 250 °C.

2.2. Chaotic mixing device

Polymers were mixed in a batch chaotic mixer (Fig. 2(a)). The cross-sectional shape of the mixing chamber (Fig. 2(b)) is similar to that of twin-screw extruders and was chosen to eliminate the zones of very low stretching and to avoid early breakup of fibrils into larger size droplets.

Two circular rotors of 0.0254 m diameter were used to maintain a shear gap (d) of 0.0127 m (Fig. 2(c)). This shear gap was much larger than about 0.0035 m, observed for a 30 mm Werner and Pfleiderer twin-screw extruder. The depth of the mixing chamber was 0.0127 m and approximately 33 gm of materials were produced from one experiment.

2.3. Waveforms of rotor motion and shear rate

The rotors were driven in co-rotating fashion by two separate motors. The speed of each rotor followed a sine waveform as in Eq. (1). The sine waveform provided the best results among a set of periodic and non-periodic waveforms, such as square, steady, and combinations of steady and sine waveform [48].

$$\Omega_A = \Omega\left(1 + \cos\frac{2\pi t}{T}\right) \tag{1}$$

$$\Omega_B = \Omega\left(1 - \cos\frac{2\pi t}{T}\right)$$

The rotors were rotated with angular speeds of Ω_A and Ω_B with a phase lag of 90°. The variables Ω and T in Eq. (1) denote the peak angular speed and the time-period respectively. The angular displacement of each rotor per period, θ is given below:

$$\theta = \int_0^T \Omega_A(t)\mathrm{d}t = \int_0^T \Omega_B(t)\mathrm{d}t = \Omega T \tag{2}$$

Since the ratio of shear gap and rotor radius was 1.0, the shear rate ($\dot{\gamma}$) was not constant in the gap; instead it varied from its highest value at the rotor surface to the lowest at the chamber wall. The peak values of shear rate at the rotor surface and at the chamber walls were respectively 17.7 and 7.1 s^{-1} for a peak rotor speed of 0.14 m/s used in this study. Accordingly, the time-averaged shear rates at the rotor surface ($\dot{\gamma}_{rotor}$) and chamber walls were respectively, 8.8 and 3.5 s^{-1}. Arithmetic mean of these shear rates, 6.15 s^{-1} was used in calculation of equilibrium size of droplets. The results presented in this study correspond to $\theta = 1440°$ with $T = 4.7$ s; a widespread mixing was produced in the entire mixing chamber for this set of parameters [47]. The value of total strain (γ) imparted by each rotor on the polymers was used to follow morphology development and was determined from $\gamma = nT\dot{\gamma}_{rotor}$, where n is the number of periods. The forcing function in Eq. (1) utilized the shear-thinning behavior of the PP-phase. For example, the shear viscosity of the PP-phase (PP2) varied from 3137 Pa s at $\dot{\gamma} = 0$ s^{-1} to 850 Pa s at $\dot{\gamma} = 6.2$ s^{-1} to 800 Pa s at $\dot{\gamma} = 7.1$ s^{-1} to 600 Pa s at $\dot{\gamma} = 17.7$ s^{-1}, while the shear viscosity of the PA6-phase remained constant at 323 Pa s.

Table 1
Weight percent of PP-phase in lamellar and fibrillar forms with variation of mixing strain for three values of zero-shear viscosity ratio (p)

Total strain (γ)	$p = 0.8$		$p = 9.8$		$p = 30$	
	10 wt% PP	30 wt% PP	10 wt% PP	30 wt% PP	10 wt% PP	30 wt% PP
167	67	84	70	85	84	95
341	36	58	42	78	82	85
667	11	43	26	54	51	73
1334	5	24	14	41	24	57
2662	2	12	4	24	10	45
5320	1	7	3	11	9	31

2.4. Mixing experiments

The pellets of polymers, approximately 0.002 m in diameter and 0.004 m in length, were added separately into designated zones of the mixing chamber to fill the volume and allowed to melt at 250 °C. A 1000-watt band heater surrounding the mixing chamber provided fast heating of polymers. A flush-mounted thermocouple on the top cover of the mixing chamber measured the melt temperature and was used to control the heating rate of the polymer. The polymer components were kept segregated until mixing began.

The results presented in this paper were obtained by mixing a block of size 0.0127 m × 0.0354 m × 0.0127 m

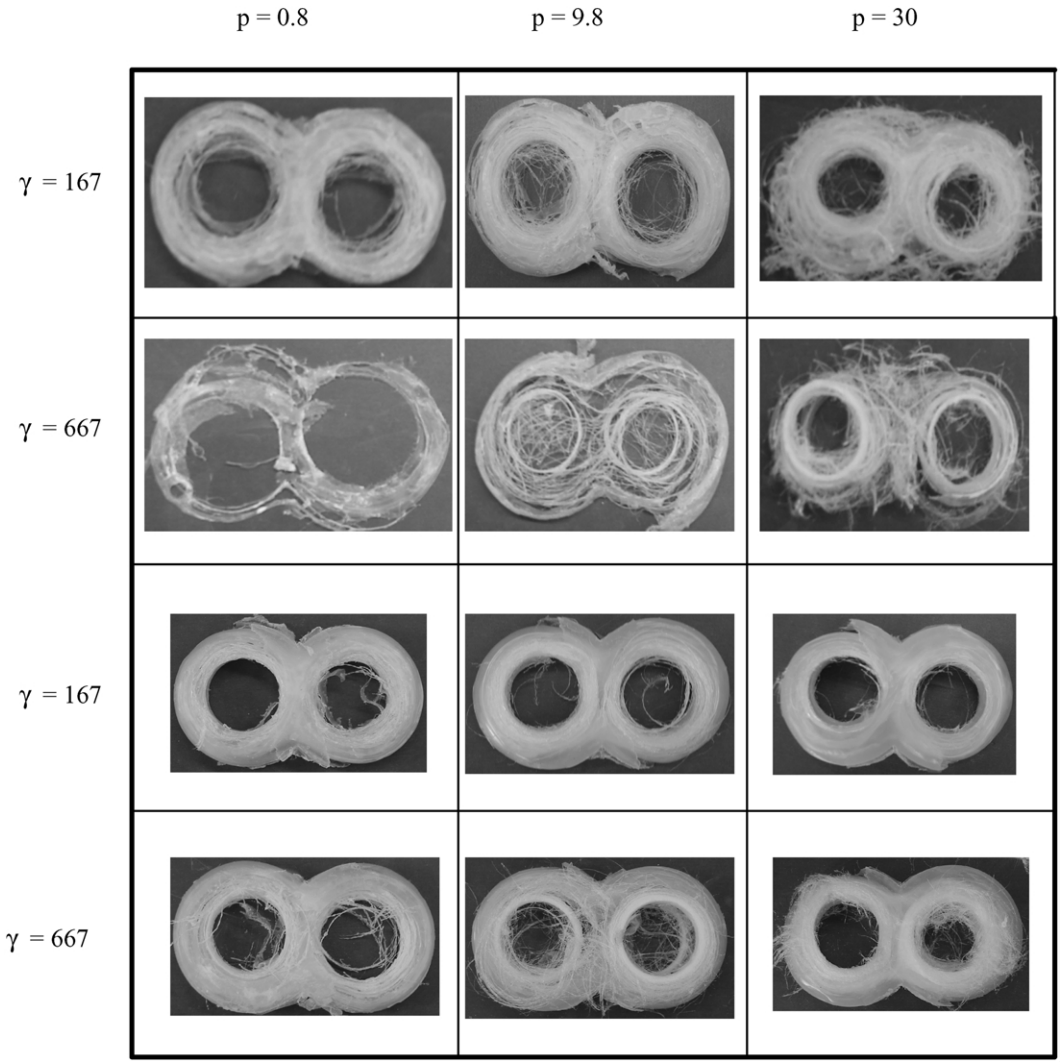

Fig. 3. Optical images of layers and fibrils of the PP-phase for p of 0.8, 9.8, and 30 at various strains (γ). The top two rows represent 10 wt% of PP-phase and the bottom two rows represent 30 wt% PP-phase in the blend.

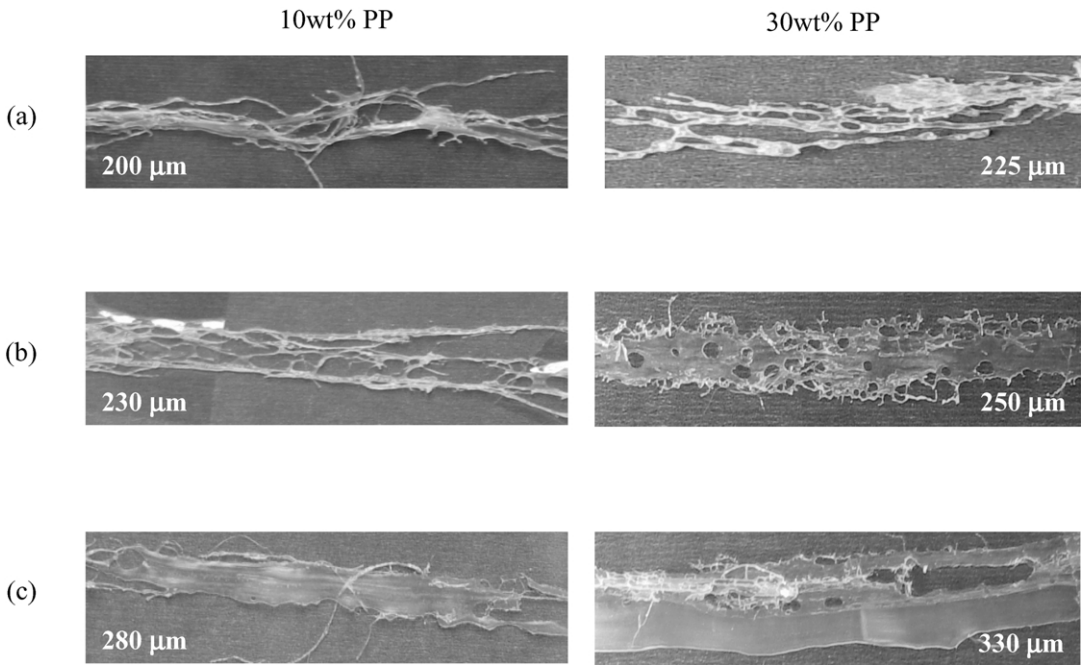

Fig. 4. Optical images of a layer collected from the rotor surface at a strain of 167. (a) $p = 0.8$, (b) $p = 9.8$, and (c) $p = 30$. Lamella thickness in each case is shown.

formed by pouring PP pellets into the narrowest zone between the rotors (Fig. 2(c)). The pellets of PA6 took approximately 5 min to melt at 250 °C; PP-pellets melted much earlier. The molten polymers were mixed for a desired total strain, after which the heater was disconnected and the mixing chamber was cooled using air jet, removed, and placed in a bath of iced water. The total times for cooling of the system to below the melting point of PP (165 °C) and to room temperature were approximately 30 s and 3 min. The top and bottom enclosures were then opened and mixed materials were collected as solid blocks for analysis. The morphology of the PP-phase was revealed by dissolving the PA6-phase in formic acid in a soxhlet extraction set up. Ceramic thimbles with nominal pore size of less than 0.1 μm were used for this purpose. The dispersed phase morphology was examined by optical and scanning electron microscope (SEM). The distributions of size of the PP domains, especially droplets, were generated using several SEM images taken for each experiment. Scion Image, image analysis software, version 4.0.2, was used for the purpose. At least 1000 droplets were used in determining the droplet size distributions.

3. Results and discussion

3.1. Morphological transitions

The dispersed phase morphology and morphological makeup of the dispersed phase, for example, the fractions of lamellas, fibrils, and droplets were obtained by extraction of the PA6-phase. Table 1 presents the weight percent of the original amount of PP remaining in lamellar and fibrillar form at different total strain; the rest of the material transformed into droplets upon breakup of the fibrils. The optical micrographs of the fractions remaining as lamella and fibrils at each stage of mixing for three grades of PP are presented in Fig. 3. These images provide clear indication whether the fractions not converted into droplets are mostly lamellas or mostly fibrils. For example, at a strain of 667, the PP-phase in 10 wt% blend was mostly fibrillar, while it was mostly lamellar in 30 wt% blend.

The trend of conversion of PP-phase into droplets for both 10 and 30 wt% blends is similar (Table 1). For example, the conversion is the slowest for $p = 30$ (PP1) and the fastest for $p = 0.8$ (PP3). However, the 30 wt% blend showed slower conversion of PP into droplets. It was found at a strain of 5320 that for $p = 0.8$, approximately 1 wt% of PP in 10 wt% blend remained as lamella, while 7 wt% of the PP-phase in 30 wt% blend remained as a combination of thick lamella and fibrils (Table 1). Similar trends were observed for other grades of PP.

A discussion is now in order on the role of viscosity ratio on the speed of conversion of PP-phase into droplets. It is intuitive that the length scale reduction in lamellar and fibrillar states is slower due to higher viscosity of the dispersed phase than the matrix. The continuity of shear stress at the interfaces can be invoked to rationalize this. In addition, the growth of interfacial instability in the lamellar structures and in extended fibrils also slows down due to higher viscosity of the dispersed phase. The characteristic

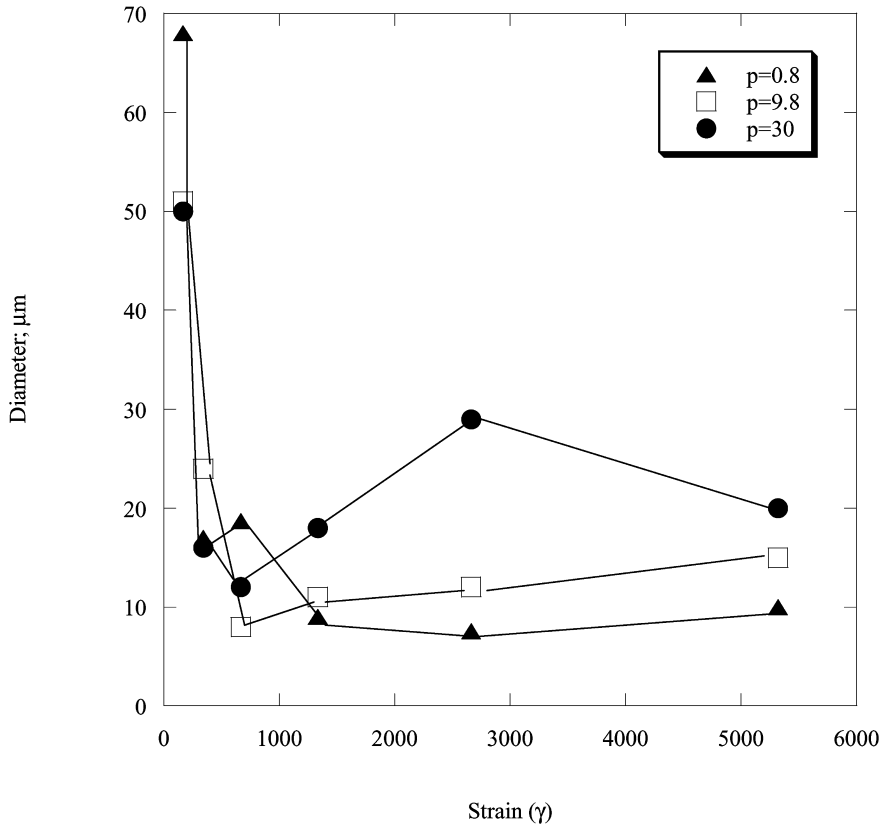

Fig. 5. Number average drop diameter versus total strain with variation of p for 10 wt% PP in blend. Solid lines represent interpolation of data points.

speed of interfacial tension driven changes is given by

$$u_\sigma = \frac{\sigma}{\eta_{0,\mathrm{PA6}}(1+p)}, \tag{3}$$

which shows an inverse relationship with the viscosity ratio, p [27]. In view of these, the lamellas were to be thickest and the interfacial instabilities were to be slowest in the case of PP1. This is clearly evident from a closer inspection of the *surviving* lamellas collected from around the rotors at a strain of 167 for three values of p (Fig. 4). It is seen that the thickness of the *thickest part* of the surviving lamellas in Fig. 4 varies from 200 μm for PP3 to 230 μm for PP2 to 280 μm for PP1 for 10 wt% blend and 225 μm for PP3 to 250 μm for PP2 and 330 μm for PP3 in 30 wt% blend. Note that identical initial conditions were used, i.e. the same size of PP-phase was placed at the same location in each experiment. In the case of 10 wt% blend, the lamellas of PP3 and PP2 developed numerous holes and even fibrils (Fig. 4(a) and (b)), while the lamella of PP1 (Fig. 4(c)) did not undergo appreciable instability due to higher viscosity of the PP-phase. In addition, while numerous small diameter fibrils can be observed in the case of PP3 (Fig. 4(a)), the handful of fibrils observed for PP1 (Fig. 4(c)) are of much larger diameter. Therefore, it can be inferred that deformation was the slowest for highest viscosity PP1, which led to delayed transition into fibrils and formation of droplets.

The fastest deformation observed in the case of PP3 can be attributed to closeness of viscosities of the PP and PA6 phases, which also offered faster growth of interfacial instabilities. The effect of viscosity ratio on the onset of instability in the lamella for 30 wt% blend followed similar trend (Fig. 4), although hole formation was delayed and the holes were much smaller compared to 10 wt% blend. It will be seen later that apart from slower morphology development at higher fractions of PP phase, much larger droplets were also formed.

3.2. Droplets above and below the equilibrium

The droplets were generated through breakup of extended fibrils by capillary instability [22,23]. Since the fibrils were formed from the lamellas and not through deformation of large mother droplets considered by other researchers [25–27], it is interesting first to check how the sizes of the droplets compare with the equilibrium size possible.

The *equilibrium diameter* (d_{eq}) in this study corresponds to droplets, which do not undergo further deformation once they are formed by coalescence from droplets of sizes smaller than d_{eq} and by breakup of droplets of sizes larger than d_{eq}. We used the Grace curve, Fig. 5 in Ref. [24] for estimates of critical capillary number for a given viscosity ratio. For this purpose, the values of viscosity ratio were calculated at a mean value of shear rate, 6.15 s^{-1}, e. g. 2.7

Table 2
Minimum and maximum droplet diameter for three values of p, produced in blends containing 10 and 30 wt% PP

Total strain (γ)	$p = 0.8$				$p = 9.8$				$p = 30$			
	10 wt%		30 wt%		10 wt%		30 wt%		10 wt%		30 wt%	
	Min (μm)	Max (μm)	Min (μm)	Max (μm)	Min (μm)	Max (μm)	Min (μm)	Max (μm)	Min (μm)	Max (μm)	Min (μm)	Max (μm)
167	7	564	11	512	2	324	2	333	7	318	5	272
341	1	131	2	564	0.5	243	2	239	1	149	3	148
667	1	179	2	461	1	59	2	312	1	72	7	180
1334	2	62	3	336	1	65	1	439	1	186	6	272
2662	0.5	37	1	315	1	112	1	271	6	300	4	125
5320	2	31	2	255	1	115	1	66	1	294	4	183

for PP2/PA6 and 0.6 for PP3/PA6 system. The corresponding estimated critical capillary numbers were 7 and 1 and the values of d_{eq} were 78 and 12 μm, respectively. Note that for PP1/PA6 system, the viscosity ratio was approximately 8.7 at the mean shear rate of 6.15 s^{-1} and the Grace curve indicates a critical capillary number much greater than 100. In view of this, the value of d_{eq} for $p = 30$ was not estimated from the Grace curve. Another point to note is that the values of d_{eq} calculated from the critical capillary numbers represent the largest stable droplets.

Table 2 lists the minimum and maximum droplet diameter observed in each case. It is worthwhile to mention that in each case, the minimum size droplets constituted approximately 2–4% of the droplet population, while in all cases, 1 or 2 largest size droplets were found in a population of approximately 1000 droplets. The minimum droplet diameter fell in the range 1–11 μm, while the maximum droplet diameter varied between 59–564 μm.

Tables 3 and 4 present a breakdown of the total population of droplets smaller and greater than the equilibrium size d_{eq} at the mean shear rate of 6.15 s^{-1}. For the 10 wt% blend, at a strain of 5320, it is seen that approximately 72 and 99.7% of the droplet population fell below the equilibrium size with the number average size of respectively, 7 and 16 μm for $p = 0.8$ and 9.8. The number average size of entire droplet population for $p = 30$ was 33 μm.

Much smaller fractions of droplets fell below the equilibrium size for $p = 0.8$ at the same strain for the 30 wt% blend, e.g. 32% with the number average droplet diameter of 8 μm. Note that the number average sizes of the fractions smaller than the equilibrium size are approximately $1/10 - 1/2$ the equilibrium size, thus endorsing the suitability of chaotic mixing as a means for dramatic size reduction.

Despite large populations of droplets falling below the equilibrium size, the presence of a few very large size droplets in each case skewed the volume fraction figures in Tables 3 and 4. For example, in the case of 30 wt% blend (Table 4), the volume of fractions below the equilibrium size accounted for only 0.4% of droplet volume for $p = 0.8$. Looking at Table 2, it is evident that the largest size droplets, although a few in number, contributed to the volume significantly, e.g. a 255 μm droplet at $\gamma = 5320$ contributes $\sim$10,000 times the volume of one 12 μm droplet. These large droplets may have been generated through breakup of larger diameter fibrils or at later periods through repeated coalescence of midsize droplets. A reflection into Table 2 reveals that the size of largest droplets gradually decreased with

Table 3
Comparison of volume percent and number percent of drops above and below d_{eq} and their number average diameters for two values of viscosity ratios (p) with 10 wt% of PP-phase at various strain (γ)

γ	$p = 0.8$				$p = 9.8$			
	Volume (%)/(number (%))		Number average size (μm)		Volume (%)/(number (%))		Number average size (μm)	
	$< d_{eq}$	$> d_{eq}$	$< d_{eq}$	$> d_{eq}$	$< d_{eq}$	$> d_{eq}$	$< d_{eq}$	$> d_{eq}$
167	0.05/(4)	99.95/(96)	11	68	0.3/(80)	99.7/(20)	36	111
341	1/(34)	99/(66)	7	23	0.1/(92)	99.9/(8)	16	111
667	0.5/(57)	99.5/(43)	8	32	100/(100)	0/(0)	8	–
1334	9/(79)	91/(21)	7	16	100/(100)	0/(0)	11	–
2662	4/(80)	96/(20)	4	14	82/(99.9)	18/(0.1)	12	112
5320	7/(72)	93/(28)	7	18	81/(99.7)	19/(0.3)	16	105

Table 4
Comparison of volume percent and number percent of drops above and below d_{eq} and their number average diameters for two values of viscosity ratio (p) with 30 wt% of PP-phase at various strain (γ)

γ	$p = 0.8$				$p = 9.8$			
	Volume (%)/(number (%))		Number average size (μm)		Volume (%)/(number (%))		Number average size (μm)	
	$< d_{eq}$	$> d_{eq}$	$< d_{eq}$	$> d_{eq}$	$< d_{eq}$	$> d_{eq}$	$< d_{eq}$	$> d_{eq}$
167	~0/(0.7)	~100/(99.3)	11	62	16/(88)	84/(12)	21	106
341	~0/(6)	~100/(94)	8	51	13/(87)	87/(13)	23	105
667	~0/(18)	~100/(82)	8	27	3/(97)	97/(3)	8	109
1334	0.1/(21)	99.9/(79)	9	30	3/(97)	97/(3)	8	109
2662	0.2/(19)	99.8/(81)	8	24	36/(97)	64/(3)	23	105
5320	0.4/(32)	99.6/(68)	8	23	100/(100)	0/(0)	8	–

strains, thus indicating repetitive deformation and breakup. This is readily apparent in 10 wt% blend of PP3. In some cases, the size of largest droplets first decreased through repetitive breakup and then increased through coalescence, e.g. in the case of 10 wt% blend of PP2.

3.3. Breakup and coalescence

The evolution of number average diameter reflects the relative importance of breakup of fibrils and coalescence of droplets in determining the transient morphology at various stages of mixing. For example, Figs. 5 and 6 show a few transitions in the number average droplet size, especially early in mixing, for both 10 and 30 wt% blends.

As a general trend, at long mixing times, e.g. at $\gamma = 5320$ (~ 10 min), the number average diameter increased with p, as is routinely observed in the blending of immiscible polymers [49,53,54]. This, however, is contrary to what is observed in the breakup of cylindrical threads in systems with high values of interfacial tension [27]; in the latter case, much larger droplets are formed at low values of p due to low length stretching, $O(100)$ and rapid growth of interfacial instabilities leading to faster breakup. On the

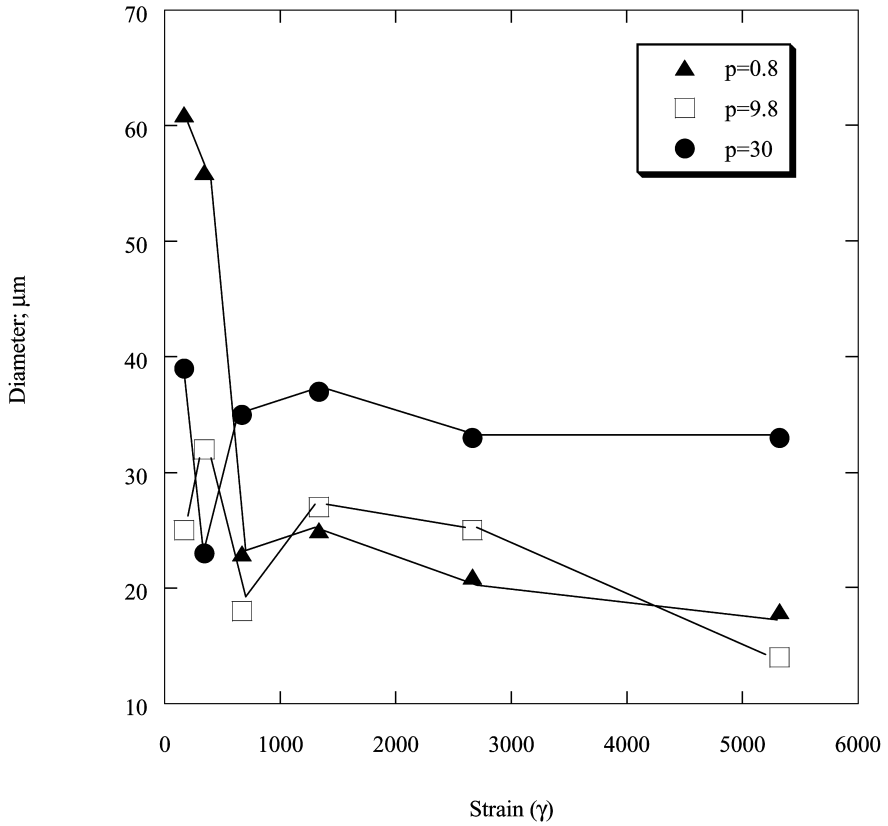

Fig. 6. Number average drop size versus total strain with variation of p for 30 wt% of PP blend. Solid lines represent interpolation of data points.

Table 5
Variation of minimum, maximum, number average, and volume average drop size with the effect of annealing at p of 9.8. 10 wt% of PP-phase was used

Total strain (γ)	Unannealed				Annealed			
	Min dia (μm)	Max dia (μm)	Volume average dia (μm)	Number average dia (μm)	Min dia (μm)	Max dia (μm)	Volume average dia (μm)	Number average dia (μm)
667	1	59	29	8	2	144	89	14
1334	1	65	33	11	1	216	120	13

other hand, liquid threads of higher viscosity undergo affine stretching to much larger length, $O(10^4)$. In addition, capillary instability is delayed due to higher viscosity (Eq. (3)). Consequently, much smaller droplets are formed [27].

The number average droplet diameter also increased as the concentration of the PP-phase increased from 10 to 30 wt%. This is in line with the findings of several investigations [51–54]. Favis [52] found that the number average diameter increases as $\sim(\phi+\phi^2)$, where ϕ is the volume fraction of the dispersed component.

The trends observed in Figs. 5 and 6 in the early stages of mixing e.g., below a strain of ~1334 (2.5 min of mixing) do not reveal any correlations between droplet sizes and viscosity ratio and composition. During this period, a large population of fibrils broke up into droplets and the rest of the fibrils experienced large stretching and went through breakup at later stages. In addition, coalescence took place especially at strains of 1334 or higher, causing coarsening of the droplet population. However, considering only the fractions of fibrils breaking very early, e.g. at or below a strain of 167, a correlation can be found. The number average size decreased with viscosity ratio, p in line with those observed in thread breakup studies [27]. At later stages, the breakup of larger diameter fibrils and coalescence added complications.

The size reduction of droplets occurred more consistently for $p = 9.8$ till coalescence became prominent at or beyond a strain of 1334 (Fig. 5). For 10 wt% blend, the number average diameter went through a minimum of 8 μm at $\gamma = 667$ and increased to 11 μm at $\gamma = 1334$. Similar trends are observed in other grades of PP for both 10 and 30 wt% blends. This increase can be due to coalescence or generation of droplets through breakup of large diameter fibrils, or both. A close inspection of Table 1 reveals that breakup of large diameter fibrils contributed to such moderate coarsening of the number average droplet size. For example, in the case of 10 wt% blend of PP2 ($p = 9.8$), the large diameter fibrils present in Fig. 3 at $\gamma = 667$ went through breakup and produced larger droplets as the droplet fraction increased from 74 to 86% between the strains of 667 and 1334. This was further confirmed by annealing the mixed materials.

In annealing experiment, mixing was stopped after a strain of 667 (75 s) and the materials were allowed to stay inside the mixing chamber under quiescent condition at 250 °C for 527 s, the same length of time that gave a strain of 5320 with continued mixing. As a result, the transient morphology, e.g. a combination of lamella, fibrils, and droplets, went through further morphological changes. It was seen that an additional 5–7 wt% of the fibrils were converted into droplets during annealing. While such observation confirms the breakup of fibrils into droplets, a more interesting observation, that of formation of larger droplets, gives credence to a hypothesis that the larger size fibrils broke up during this period (Table 5). The number average diameter of drops was seen to increase from 8 μm at strain of 667 to 14 μm due to annealing and the droplet size distribution became wider. Coalescence taking place under quiescent condition alone cannot explain such an increase in size.

Similar argument can be invoked to explain the small increase of number average droplet diameter from 17 μm at $\gamma = 341$ to 19 μm at $\gamma = 667$ for PP3 ($p = 0.8$) as in Fig. 5. In this case, the droplet fractions increased from 64 to 89% through breakup of larger diameter fibrils (Table 1). The same system shows a sharp decrease of number average droplet diameter at strain of 1334, whereby the maximum droplet size reduced from 179 μm at $\gamma = 667$ to 62 μm for $\gamma = 1334$; the number average diameter also reduced substantially from 19 to 9 μm as the fraction of droplets smaller than the equilibrium size increased from 83 to 99.8% and the fraction of PP converted into droplets increased from 57 to 79% in this period. Consequently, this size reduction must be due to further deformation and breakup of the droplets larger than the equilibrium size. Coalescence became important afterwards and coarsening of droplets occurred between the strains of 1334 and 2662 (Fig. 5).

The number average size increased by about 2 to 3-fold in the viscosity ratio range of 0.8–30 as the concentration of PP-phase was increased from 10 to 30 wt%,. For PA6/PP immiscible blend, Willis et al. [50] also reported about two folds increase in the number average size when the concentration of the minor phase was increased from 10 to 30 wt%.

3.4. Scaling of droplet size distribution

We are now in a position to inspect the scalability of droplet size distributions. Muzzio et al. [31] found that droplets produced by breakup of cylindrical threads in a chaotic flow showed scaling behavior; the droplet size

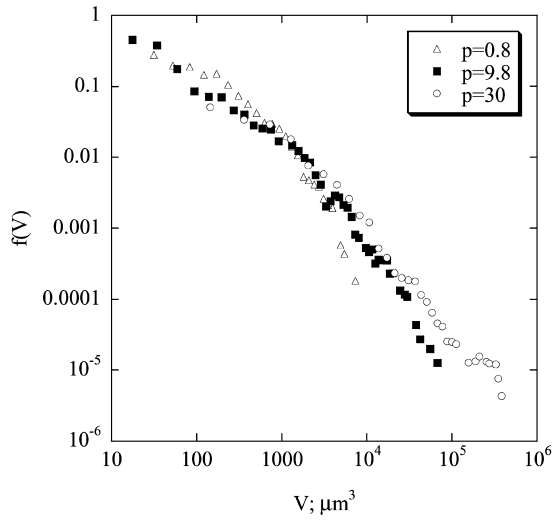

(a)

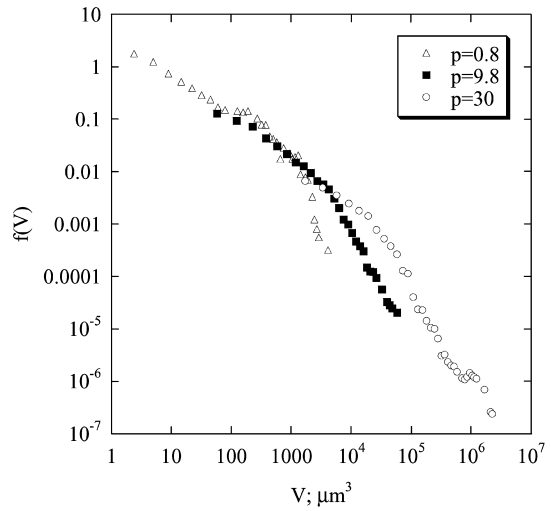

(b)

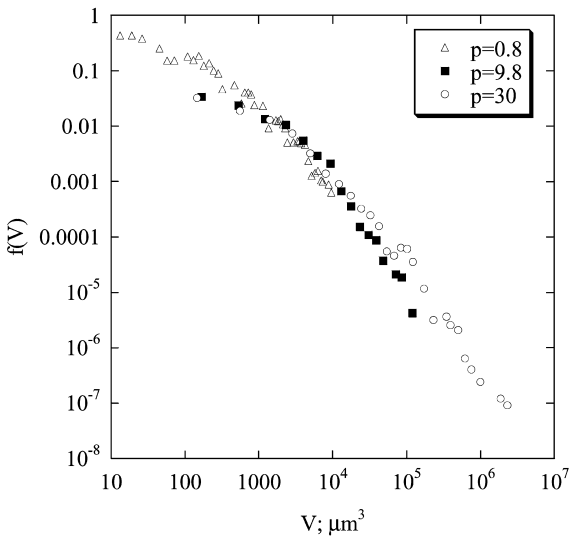

(c)

distributions upon scaling collapsed into two families of curves, depending upon the values of p. Note that stretching distribution and striation thickness distribution produced by chaotic mixing flows also show scaling features [30]. In view of this, it was anticipated that droplets produced in this study would show similar scaling features.

Figs. 7 and 8 present frequency distribution of volume (V) of droplets of various grades of PP at strains ranging from 1334 to 5320. The droplet sizes were first arranged in several bins of equal size range of diameter and the mean volume of droplets in each bin and the number of droplets in each bin was recorded. The frequency distribution $f(V)$ is defined such that $\mathrm{d}N \equiv f\,\mathrm{d}V$ droplets have volume between V and $V + \mathrm{d}V$ in a population of N droplets. In each case, 1000–1500 droplets were used to generate the frequency distribution. The data presented in Figs. 7–10 were scaled to 100 droplets. It is seen that the droplet size distribution is the narrowest for $p = 0.8$ and widest for $p = 30$ as is usually observed in polymer blending [49–54]. The distribution widened at higher values of strains as breakup of larger diameter fibrils and coalescence of smaller drops became important.

The frequency distributions presented in Fig. 8 for 30 wt% blend also reflect much larger droplets. The distributions show plateau at smaller volumes which are readily apparent at higher strains, e.g. at $\gamma = 5320$ in Figs. 7(c) and 8(c). These plateau formed by small size droplets are indicative of multiple breakups of larger droplets as originally identified by Muzzio et al. [31] in their study on breakup of extended threads in chaotic flow. In view of Figs. 7 and 8, multiple breakup in the present study correspond to breakup of droplets larger than the equilibrium size, which resulted both from breakup of fibrils early in mixing and from coalescence of smaller droplets at later stages.

The droplet size distributions of Figs. 7 and 8 are recast through proper scaling, such as $V^2 f(V)/M_1$ vs. V/V_m, where M_1 is the first moment of the distribution $f(V)$ and V_m is the mean volume of droplets determined from $V_\mathrm{m} = M_2/M_1$, with M_2 as the second moment of $f(V)$. These results are presented in Figs. 9 and 10. As is readily apparent, the distributions of Figs. 7 and 8 do not collapse into single curves in Figs. 9 and 10, even though droplets produced by thread breakup in chaotic flow exhibited such collapse [31]. The curves for $p = 0.8$, 9.8, and 30 are different and represent different families. One wonders why the droplet size distributions do not follow the same scaling as in breakup of liquid threads, while it is true that the lamellar structures and thinning fibrils follows scalability of stretching distribution. The missing link, it appears, is the process of generation of fibrils through interfacial instability in the lamellar structures.

Fig. 7. Frequency distribution of drop volumes for strains (γ) of (a) 1334, (b) 2662, and (c) 5320 for three values of viscosity ratio (p) with 10 wt% of PP-phase.

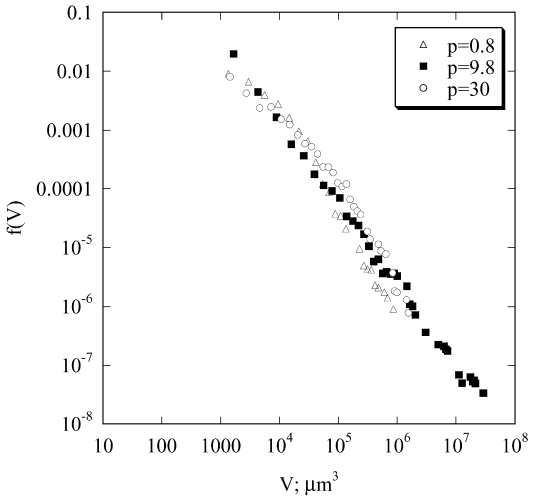

(a)

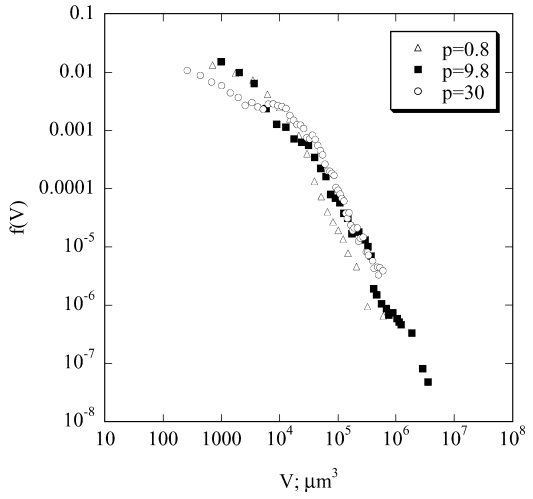

(b)

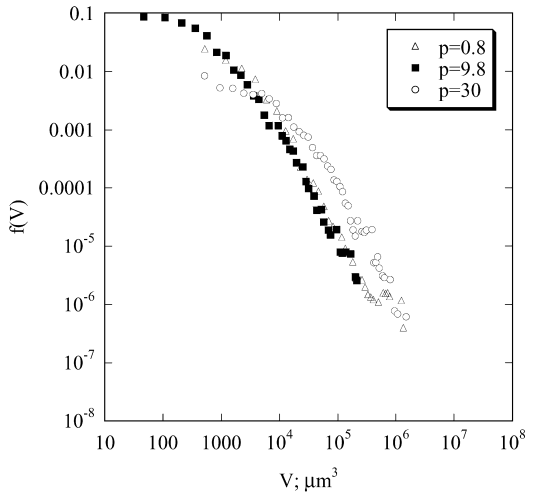

(c)

Fig. 8. Frequency distribution of drop volumes for strains (γ) of (a) 1334, (b) 2662, and (c) 5320 for three values of viscosity ratio (p) with 30 wt% of PP-phase.

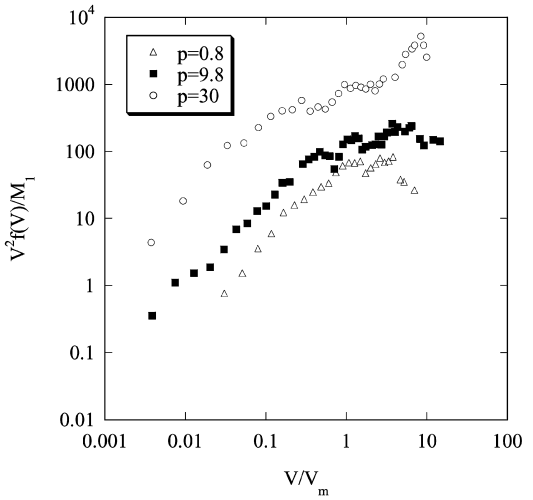

(a)

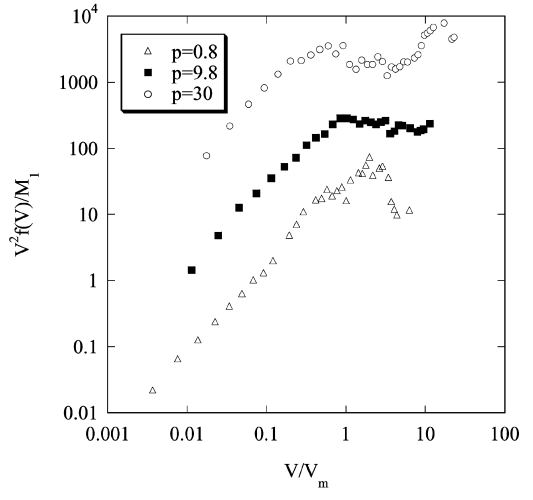

(b)

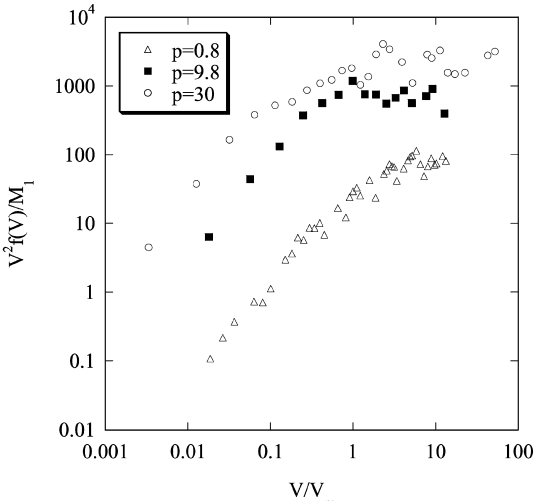

(c)

Fig. 9. Scaling of drop volumes for strains (γ) of (a) 1334, (b) 2662, and (c) 5320 for three values of viscosity ratio (p) with 10 wt% of PP-phase.

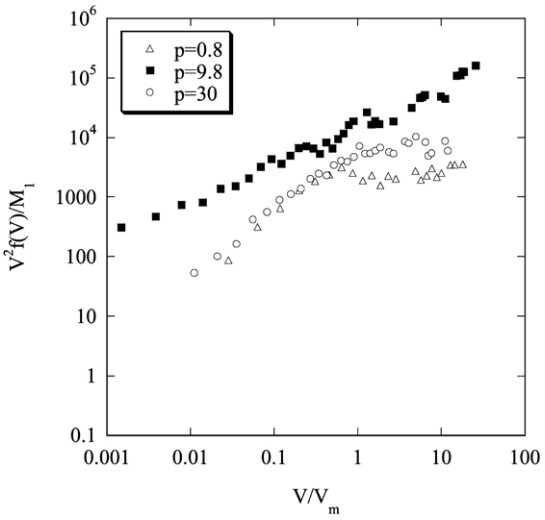

(a)

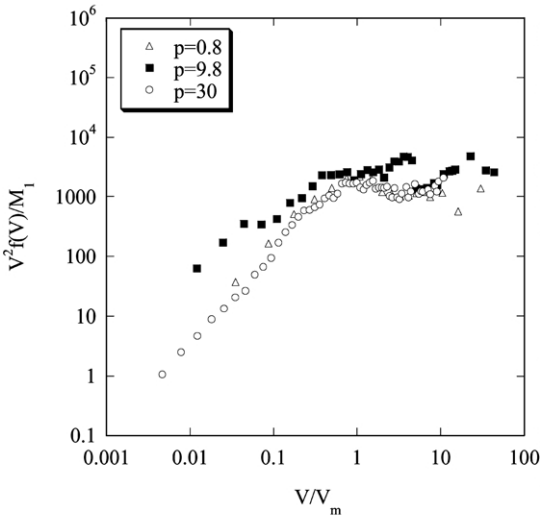

(b)

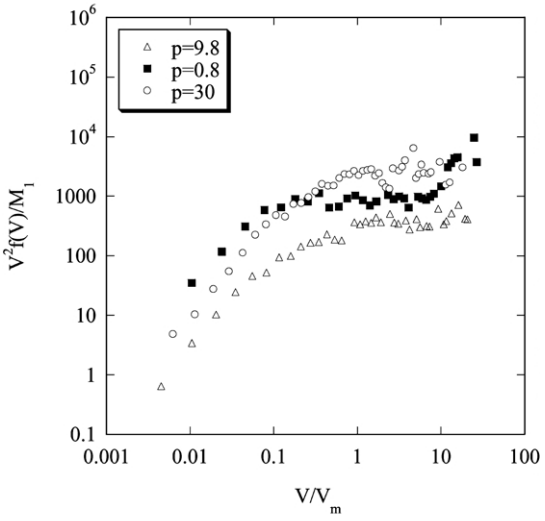

(c)

Fig. 10. Scaling of drop volumes for strains (γ) of (a) 1334, (b) 2662, and (c) 5320 for three values of viscosity ratio (p) with 30 wt% of PP-phase.

It is interesting to note that all lamellas were produced parallel to the axis of the rotors due to two-dimensional flow in the mixing device. However, as evident in Fig. 4, the instabilities leading to the formation of holes in the lamellas were not uniform along the width of the lamellas. In other words, fibrils formed at various width of the same lamella varied in diameter, with no apparent scaling features associated with their diameter, even though the thickness distribution of lamellar structures till the point of growth of instability followed scaling features. The diameter along the length of a single fibril, however, follows proper scaling commensurate with the distribution of local stretching values [27,31]. This lack of scaling of diameter in fibril population is carried over to the droplet population as well. Another factor can also be considered to interpret the absence of scaling features in Figs. 9 and 10. A fibril undergoing capillary instability may be influenced by the breakup sequence of neighboring fibrils or neighboring droplets from an earlier breakup [56,57], which is especially true at higher concentrations of the PP-phase, e.g. 30 wt%. Yet another factor might be the process of coalescence. Two neighboring drops coalescing to form a larger drop, may not follow self-similar scaling features, even though, aggregates formed by flocculation of solid particles have been shown to follow scaling behavior [58]. The hydrodynamic interactions between the droplets may be responsible for such deviation from the scaling behavior. Note that the effect of coalescence was absent in the experimental system of Muzzio et al. [31] and was not considered in the theoretical treatment in Ref. [58].

One might question the wisdom of adding PP-phase in the form of block (Fig. 2(c)) instead of in the form of premixed pellets and argue that scalability of droplet size distribution was lost due to this non-conventional initial condition. Separate experiments with premixed pellets, carried out under otherwise identical conditions, revealed that morphological developments followed the same sequence of lamella to fibrils to droplets and the droplet size distributions were similar to the ones presented in Figs. 8–10. We opted to use a segregated initial condition, as monitoring of various morphological transitions became much easier, e.g. the lamellar and fibrillar forms of the PP-phase remained connected and became apparent after dissolution of the PA6-phase.

4. Concluding remarks

This study showed that dispersive mixing of polymers is possible in shear flows for systems with high values of viscosity ratio. Although the results reported were associated with zero-shear viscosity ratio (p), the operating

viscosity ratio between PP and PA6 at a mean shear rate of 6.15 s^{-1} was approximately 10 for PP3 (Fig. 1(b)), which is much larger than a limit of 4 seen in Grace curve [24]. The initial capillary number, Ca, based on a pellet of PP of length 0.004 m and a shear rate of 6.15 s^{-1} was approximately 6000 and the shear stress was of the order of 2000 Pa, which are much larger than those encountered in the breakup of threads of low viscosity liquids. Many commercial blends are also routinely produced by screw extrusion of components with viscosity ratio much greater than 20. Some researchers attribute this to contributions from extensional flow field present in batch mixing devices and screw extruders [53,59]. As already seen, dispersion of PP in PA6 was possible and droplets of few micrometers were produced even though the flow kinematics involved only shear flow.

A two-fold increase in PP droplet size was observed for increase of p from 0.8 to 30. This dependence of droplet size on viscosity ratio is opposite of what was observed in earlier studies on thread breakup. This can be attributed to interference of breakup patterns of multiple, neighboring fibrils [56,57], elasticity of dispersed polymer [1], and coalescence. This study also showed an increase of the number average droplet size with the increase of concentration of the PP phase. The relationship between the dispersed phase size and the viscosity ratio in the context of chaotic mixing needs a thorough investigation.

It is seen that the faster rate of conversion of PP-phase from lamellas and fibrils into droplets with narrow distribution of droplet size occurred for $p = 0.8$. At higher loading, the deformation of the PP-phase was slowed down. The droplet size distribution did not follow proper scaling probably due to a lack of scalability of interfacial tension driven breakup of the lamellas. The influence of coalescence and interference of breakup process of fibrils by neighbors may also have contributed to deviation from the scaling behavior.

Acknowledgements

This work was supported by National Science Foundation in the form of CAREER Award (DMI-0134106) to SCJ.

References

[1] Van Oene H. J Colloid Interface Sci 1972;40:448–67.
[2] Ghosh AK, Ranganathan S, Lindt JT, Lorex S. SPE ANTEC Proc 1991;37:232–6.
[3] Lindt JT, Ghosh AK. Polym Engng Sci 1992;32:1802–13.
[4] Scott CE, Macosko CW. Polym Bull 1991;26:341–8.
[5] Scott CE, Macosko CW. Polymer 1995;36(461):470.
[6] Sundararaj U, Dori Y, Macosko CW. Polymer 1995;36:1957–68.
[7] Sundararaj U, Macosko CW, Rolando RJ, Chan HT. Polym Engng Sci 1992;32:1814–23.
[8] Lyngaae-Jorgensen J. J Macromol Sci Phys 1996;B35:357–73.
[9] Ottino JM, Ranz WE, Macosko CW. Chem Engng Sci 1979;34:877–90.
[10] Erwin L. Polym Engng Sci 1978;18:1044–8.
[11] Erwin L. Polym Engng Sci 1978;18:572–6.
[12] Aref H. J Fluid Mech 1984;143:1–21.
[13] Ottino JM. The kinematics of mixing: stretching, chaos, and transport. New York: Cambridge University Press; 1989.
[14] Leong CW, Ottino JM. J Fluid Mech 1989;209:463–99.
[15] Swanson PD, Ottino JM. J Fluid Mech 1990;213:227–49.
[16] Niederkorn TC, Ottino JM. J Fluid Mech 1993;256:243–68.
[17] Jana SC, Metcalfe G, Ottino JM. J Fluid Mech 1994;269:199246.
[18] Kusch HA, Ottino JM. J Fluid Mech 1992;236:319–48.
[19] Jana SC, Tjahjadi M, Ottino JM. AIChE J 1994;40:1769–81.
[20] Hwang WR, Jun HS, Kwon TH. AIChE J 2002;48:1621–30.
[21] Taylor GI. Proc R Soc London 1934;A146:501–23.
[22] Tomotika S. Proc R Soc London 1935;A150:322–37.
[23] Tomotika S. Proc R Soc London 1936;A153:302–18.
[24] Grace HP. Chem Engng Commun 1982;14:225–77.
[25] Stone HA. Ann Rev Fluid Mech 1994;26:65–102. also references there in.
[26] Khakhar DV, Ottino JM. J Fluid Mech 1986;166:265–85.
[27] Tjahjadi M, Ottino JM. J Fluid Mech 1991;232:191–219.
[28] Jenssen JMH, Meijer HEH. Polym Engng Sci 1995;35:1766–80.
[29] Chesters A. Chem Engng Res Des 1991;69A:259–70.
[30] Muzzio FJ, Swanson PD, Ottino JM. Phys Fluids A 1991;3:822–34.
[31] Muzzio JF, Tjahjadi M, Ottino JM. Phys Rev Lett 1991;67:54–7.
[32] Muzzio FJ, Liu M. Chem Engng J (Lausanne) 1996;64:117–27.
[33] Metcalfe G, Ottino JM. Phys Rev Lett 1994;72:2875–8.
[34] Szalai ES, Kukura J, Arratia PE, Muzzio FJ. AIChE J 2003;49:168–79.
[35] Galaktionov OS, Anderson PD, Peters GWM, Meijer HEH. Can J Chem Engng 2002;80:604–13.
[36] Kruijt PGM, Galaktionov OS, Anderson PD, Peters GWM, Meijer HEM. AIChE J 2001;47:1005–15.
[37] Zumbrunnen DA, Miles KC, Liu YH. Composites Part A 1996;27A:37–47.
[38] Liu YH, Zumbrunnen DA. J Mater Sci 1999;34:1921–31.
[39] Kwon O, Zumbrunnen DA. J Appl Polym Sci 2001;82:1569–79.
[40] Zumbrunnen DA, Inamdar S. Chem Engng Sci 2001;56:3893–7.
[41] Zumbrunnen DA, Chhiber C. Polymer 2002;43:3267–77.
[42] Tjahjadi M, Foster RW. US Patent No. 5551777; 1996.
[43] Jana SC, Scott E, Sundararaj UT. US Patent No. 6132076; 1998.
[44] Hwang WR, Jun HS, Kwon TH. AIChE J 2002;48:1621–30.
[45] Kim SJ, Kwon TH. Adv Polym Technol 1996;15:4154.
[46] Kim SJ, Kwon TH. Adv Polym Technol 1996;15:55–69.
[47] Sau M, Jana SC. Polym Engng Sci 2003; in press.
[48] Sau M, Jana SC. AIChE J. Submitted for publication.
[49] Wu S. Polym Engng Sci 1987;27:335–43.
[50] Willis JM, Caldas V, Favis BD. J Mater Sci 1991;26:4742–50.
[51] Favis BD, Chalifoux JP. Polymer 1988;29:1761–7.
[52] Favis BD, Willis JM. J Polym Sci: Part B: Polym Phys 1990;28:2259–69.
[53] Favis BD, Chalifoux JP. Polym Engng Sci 1987;27:1591–600.
[54] Serpe G, Jarrin J, Dawans F. Polym Engng Sci 1990;30:553–65.
[55] Chappelear DC. Polym Prepr 1964;5:363–71.
[56] Elemens PHM, van Wunnik JM, van Dam RA. AIChE J 1997;43:1649–51.
[57] Knops YMM, Slot JJM, Elemans PHM, Bulters MJH. AIChE J 2001;47:1740–5.
[58] Muzzio FJ, Ottino JM. Phys Rev A 1988;38:2516–24.
[59] Stegeman YW, van de Vosse FN, Meijer HEH, Can. J Chem Engng 2002;80:632–7.